ACS APPLIED MATERIALS & INTERFACES

Research Article

www.acsami.org

Thermal Transfer in Graphene-Interfaced Materials: Contact Resistance and Interface Engineering

Hanxiong Wang,[†,‡] Jixuan Gong,[†,‡] Yongmao Pei,*[,†] and Zhiping Xu*[,‡]

[†]State Key Lab for Turbulence and Complex Systems, College of Engineering, Peking University, Beijing 100871, China

[‡]Department of Engineering Mechanics and Center for Nano and Micro Mechanics, Tsinghua University, Beijing 100084, China

ABSTRACT: We investigate here heat transfer across interfaces consisting of single- and few-layer graphene sheets between silicon carbides by performing nonequilibrium molecular dynamics simulations. The interfacial thermal conducitivity κ_I is calculated by considering graphene layers as an interfacial phase. The results indicate that κ_I decreases with its thickness and heat flux but increases with the environmental temperature. Interface engineering of κ_I is explored by intercalating molecules between graphene layers. These guest molecules decouple electronic states across the interface, but tune κ_I slightly, leading to a thermally transparent but electronically insulating interface. These results provide a fundamental understanding in thermal transport across weakly bound interfaces, and design recipes for multifunctional thermal interface materials, composites and thermal management in graphene-based devices.

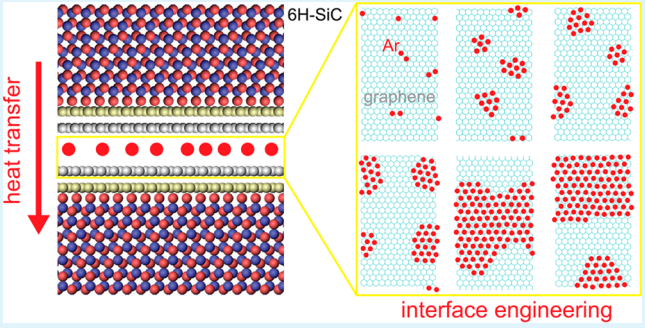

KEYWORDS: *graphene, interfacial thermal transfer, interface engineering, thermal interface materials*

INTRODUCTION

Nanomaterials and materials with nanostructured interfaces have attracted noticeable attention in recent years. Key significance of them includes high surface-to-volume ratio that leads to considerable portion of materials characterized as surfaces or interfaces and extreme exposure of atoms to the environment. These nanoscale structures can be further engineered to tune materials properties. When nanostructures are synthesized into isolated phases, aggregates, or as intercalations, size effects are unavoidably embedded. Properties of materials adjacent to the surface or interface differ from those in the bulk phase. Recent progresses in nanomanipulating and chemical functionalization techniques provide emerging opportunities in engineering surfaces or interfaces of materials down to the nanoscale,[1] which lay the ground for a new perspective of materials and device design.

As a two-dimensional material, graphene features single atomic layer thickness and holds great promises in future electronics and thermal management applications because of its outstanding electrical[2,3] and thermal properties,[4,5] as reviewed recently by Pop, Varshney, and Roy.[6] Various applications have thus been proposed, ranging from integrated circuits, nanoelectromechanical systems, to functional composites. As the characteristic dimension of materials shrinks down in these applications, local heating of materials could commonly be induced with very high intensity from electronic heating or mechanical energy dissipation, creating so-called "hot spots". To avoid the breakdown of their performance or even materials failure, the heat generated must be dissipated efficiently into a sink or the environment. This could be achieved, for example by utilizing optimally designed nanostructures.[7] In typical nanoelectronic device setups, graphene, carbon nanotubes, or other nanostructures are usually supported by a substrate, and sandwiched between two electrodes. Heat dissipation in these setups is critically defined by the efficiency of heat migration across their interfaces. A recent report pointed out that in a graphene field-effect transistor (FET), 77% of the power is dissipated through interfaces between the graphene sheet and SiO_2 substrate.[8] Thus, the design of a thermally transparent but electronically insulating interface holds the key to ensure high performance of nanoelectronics with a wide safety window.[9]

On the other hand, the interfaces between graphene and other materials also renormalize the performance of their hybrids, especially in mechanical and thermal applications. For instance, graphene and carbon nanotubes are proposed as thermal interface materials (TIM)[10] and reinforced phases in functional nanocomposites. However, the thermal conductivity of polymer-based matrix composites with graphene and carbon nanotubes as reinforcing phases shows only modest increase over the intrinsic value of polymer matrix despite the fact that these carbon nanostructures are excellent thermal conductors with high aspect ratios.[11] The performance, expected to be additive, is however strongly limited by low interfacial thermal conductivities across the weakly bonded interfaces, for example with van der Waals interactions or low-density interfacial cross-links.

Received: December 28, 2012
Accepted: March 6, 2013
Published: March 6, 2013

Therefore, to understand the nature of interfacial thermal transfer and how engineering atomic structures could modify heat conduction at these interfaces form the basis in improving performance of aforementioned applications. In addition to recent efforts in resolving detailed heat transport dynamics by experiments[12] and measuring interfacial thermal conductivities,[13] atomistic simulations show remarkably abilities in mapping interfacial nanostructures and interactions into key factors defining the thermal transport characteristics, such as thermal conductivities and energy dissipation.[9] For example, contact resistance between graphene, carbon nanotubes, and possible improvement by polymer wrapping and metal binding were investigated by atomistic simulations.[11] Hu et al. reported simulations to elucidate how interfacial thermal conductance depends on the stiffness of bulk materials and bond strength of the interface.[14] Ong and Pop examined thermal transport through the interface where carbon nanotubes is supported by a SiO_2 substrate.[15] They find that the interfacial thermal boundary conductivity scales proportionally with the strength of the van der Waals interaction, with carbon nanotube diameter, and as power law of temperature ($\sim T^{1/3}$ between 200 and 600 K). Furthermore, they find that heat dissipation into single crystal quartz and amorphous SiO_2 is similar.[16]

The interfacial thermal conductivity or contact conductivity κ_I, also known as the Kapitza conductivity, is defined according to $J/A = \kappa_I \Delta T$, where J is the heat flux across the interface, A is the cross section area, and ΔT is the temperature jump across interfaces with the assumption that effective thermal conductivity of the interface phase $\kappa_I h$ is much lower than the values of bulk materials at both sides. The width of temperature drop ΔT defines effective thickness h of the interface that could differ from the measurement of atomic positions in materials due to strong interfacial scattering of phonons.[17] The values of κ_I, as calculated or measured for different interfaces with graphene, are thus informative in designing functional devices and materials with optimal performance through effective models.

In this work, we perform nonequilibrium molecular dynamics (NEMD) simulations to explore the atomistic mechanisms of thermal transfer at interfaces between silicon carbide (SiC) and graphene. We consider both single and multiple layers of graphene sheets, where the effect of interfacial thickness h (or number of graphene layers N) is investigated. The dependence of κ_I on temperature T and heat flux J across the interface is also discussed. To explore the opportunity of interface engineering at nanoscale in tuning thermal transfer behaviors, we modify the interface by intercalating guest atoms, taking argon as an example here, and investigate their effects on interfacial thermal conduction.

MATERIALS AND METHODS

The interface between graphene and 6H-SiC is constructed at a C-terminated $(000\bar{1})$ SiC surface, which reconstructs as $(3\sqrt{3} \times 3\sqrt{3})R30°$ and coincides with a 13 × 13 graphene supercell. In our model for the interface between graphene and silicon carbide, graphene layers are sandwiched between buffer carbon layers in the bulk 6H-SiC materials, interacting through van der Waals interactions. The whole system consists of 40 000 atoms. All MD simulations are performed using the large-scale atomic/molecular massively parallel simulator (LAMMPS).[18] The time step for integrating Newtonian equations of motion is 0.2 fs, which is tested to ensure energy conservation and give a converged prediction for thermal conductivities. NEMD simulations following the Müller−Plathe approach are performed for thermal transport calculations,[19] that is, heat flux across the interface is created by inducing infrequent elastic collisions between the hot and cold regions in the system, and the temperature profile is measured after the steady state is reached.

Different numbers of graphene layers in the AB stacking order are studied. Periodic boundary conditions are applied to all directions, with lateral dimensions (x, y) of 3.2 × 5.54 nm^2 and a length of 25 nm along the direction in parallel to the heat flux and perpendicular to the interface (z). The distance between silicon atoms and the buffer layer is relaxed to be 0.2 nm, and the interlayer distance between graphene layers is 0.32 nm. To calculate temperature distribution in this hybrid system, spatial average is done for the kinetic energy and temperature of atoms along the z direction. Thermal conductivities calculated from atomistic simulation depend on the size of the hybrid system as it is usually much shorter than the phonon mean free path l_p.[20] However, as we are focusing on the heat transfer across the interface between graphene and 6H-SiC, this size effect is not expected to have significant impact, as verified by performing additional MD simulations on larger supercells.

The interatomic interactions in 6H-SiC and supported graphene are described using Tersoff[21] and adaptive intermolecular reactive empirical bond order (AIREBO) potential functions, respectively.[22,23] Noncovalent van der Waals interactions between the graphene sheet and the 6H-SiC substrate (including the buffer carbon layer) are calculated using a Lennard-Jones type of function with parameters σ_{C-C} = 0.3234 nm and ε_{C-C} = 0.00313 eV.[24] The Tersoff and AIREBO potential functions and parameters are known to be able to predict structural, mechanical and thermal properties of both silicon carbide and carbon nanostructures.[25,26] When argon atoms are intercalated between the supported and buffer layers in the simulations, a Lennard-Jones potential function with parameters ε_{Ar-Ar} = 0.3405 nm and σ_{Ar-Ar} = 0.0103235 eV is used for the Ar−Ar interaction. Simple mixing rules are used to model the interactions between argon and carbon atoms, that is, $\varepsilon_{C-Ar} = (\varepsilon_{C-C}\varepsilon_{Ar-Ar})^{1/2}$ and $\sigma_{C-Ar} = (\sigma_{C-C} + \sigma_{Ar-Ar})/2$.

We first equilibrate the system by coupling to a Berendsen thermostat at temperature T and a barostat at 1 atm. Damping time constants τ for the temperature and pressure coupling are set to 0.1 and 1 ns, respectively. Then infrequent elastic collisions are introduced to generate heat flux through the sample along the z direction. By tuning the frequency of collision ν, a final temperature difference between the hottest and cold regions is controlled to be below 100 K. The heat flux $J = Q/A\Delta t$ converges to a constant within a few nanoseconds, where Q is the energy in and out flow in the hot and cold region within a time interval Δt, respectively.

RESULTS AND DISCUSSION

Effects of the Thickness of Graphene Layers. Considering graphene layers or graphite nanoplatelets as interfacial phases in materials, the interfacial thermal conductivities across the graphene layers sandwiched between 6H-SiC are shown in Figure 1. The Kapitza conductivity or interfacial thermal conductivity is defined as $\kappa_I = J/(A\Delta T)$, where ΔT is the temperature difference between two sides of the interfacial phase including both the buffer layer and underlying SiC materials for this specific system. The values of κ_I are calculated to be 0.101, 0.09, 0.082, and 0.072 GW m^{-2} K^{-1}, respectively, for N (= 1, 2, 3, and 4) graphene layers. These results clearly show that as the number of graphene layers, or thickness of the interfacial phase increases, κ_I keeps decreasing linearly. Similar thickness dependence was reported for Au/Ti/N-layer graphene/SiO_2 by time-domain thermoreflectance (TDTR) measurement using laser beams.[13] Although the materials are quite different from our graphene-6H-SiC system, the underline mechanisms are the same. Koh et al. observed also that κ_I decreases when N increases, on the order of 0.025 GW m^{-2} K^{-1}.[13] The higher values of κ_I measured in our systems could result from the "more perfect" interfaces here

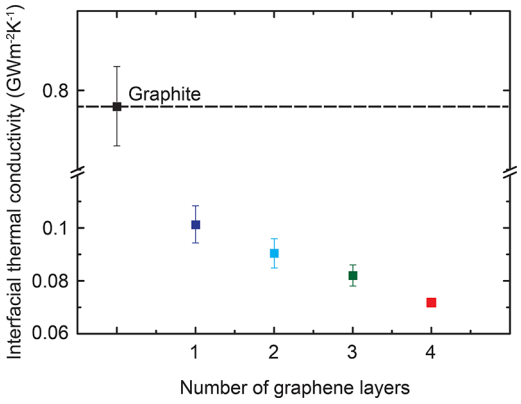

Figure 1. Interfacial thermal conductivity κ_I of N graphene layers, which are considered as an interfacial phase between 6H-SiC with buffer layer surfaces. The value of κ_I for graphite is also plotted for reference. Error bars show averaged values and standard deviations of κ_I from 3 independent runs.

between graphene and buffer layers in silicon carbides, which is in registry. Phonon modes matching and their transmission are thus enhanced across the interface here. Temperature distribution in the system shows that the temperature gradients in graphene layers and silicon carbide are significantly lower than that in the interface, that is, between graphene layers and the buffer carbon layers as the surfaces of 6H-SiC. This suggests that the contact resistance R_c at the interface plays a dominant role in heat transfer. For $N < 5$, our simulation results can be approximately fitted by a linear function $\kappa_I = -0.095N + 0.11$ to the number of graphene layers N in unit of GW m^{-2} K^{-1}. For higher N values, κ_I will gradually decays to zero.

To interpret the linear dependence of κ_I on N, we describe here a simple chain model of thermal resistors by assuming a diffusive transport mechanism across the interfaces. As illustrated in Figure 2, we consider the hybrid system as a

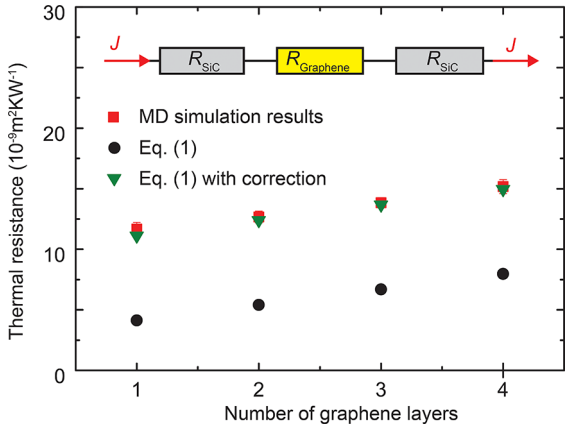

Figure 2. Effective thermal resistance R as calculated from MD simulation results (squares). Predictions from the one-dimensional resistor-chain model are also plotted with (triangles) and without (circles) consideration of the contact resistance.

serial sequence of three independent resistors with individual thermal resistance R_{SiC1}, $R_{graphene}$, and R_{SiC2}, respectively, where $R = L\kappa^{-1}A^{-1}$ is the equivalent resistance of a resistor with thermal conductivity κ, length L, and cross-section area A. The effective thermal resistance of the entire system is

$$R = R_{SiC1} + R_{graphene} + R_{SiC2} \quad (1)$$

In our simulations, silicon carbides, represented by R_{SiC1} and R_{SiC2}, at each side of the interface are symmetrically aligned. We determine the values of thermal resistance from bulk thermal conductivities of graphene and silicon carbides in perpendicular to the interface (z direction), which are calculated here through MD simulations. The predictions using the equivalent thermal resistor model are plotted in Figure 2, which are further compared to simulation results from NEMD simulations. It is found that a correction by including two additional interfacial thermal resistors is required, with total thermal resistance from two contacts $2R_c = 7.303$ nW^{-1} m^2 K, to obtain a consistent prediction. Our simulation results show that the two contact resistors are identical because of the limited amplitude of heat flux and temperature difference across the contacts. The value of R_c obtained here is also consistent with experimental measurements of contact resistance in other interfaces with graphene, on the order of 10 nW^{-1} m^2 K, as summarized in ref 6. As R increases with N, this correction becomes negligible for large N, but significant for few-layer graphene as investigated in our simulations ($N < 5$). The interfacial thermal conductivity could thus be calculated from $R_{graphene}$ and R_c, that is

$$\kappa_I = 1/[(R_{graphene} + 2R_c)A] \quad (2)$$

Because $R_{graphene}$ scales linearly with N, κ_I will scale as $1/(N + c)$, where c is a constant. This function can be fitted into a linear function for small N, then decreases to zero, as we observed from simulation results.

Effect of Heat Flux and Environmental Temperature. Our simulation results show that heat flux across the interface has significant impact on the interfacial thermal conductivity κ_I. In our NEMD simulations, the frequency of momentum exchange between atoms in the hot and cold reservoir can be changed here to tune the amplitude of heat flux. We consider this effect by exploring systems equilibrated at 300 and 600 K, respectively. The results are shown in Figure 3, which suggest that κ_I decreases with the heat flux at both environmental temperatures, and the decrease tendency is weakened at 600 K than 300 K.

Moreover, we conclude from Figure 3 that the interfacial thermal conductivity also depends on the environmental temperature, that is, κ_c increases with T at the same heat flux that agrees with Koh et al.'s measurement for graphene,[6] and Ong and Pop's simulation results for carbon nanotubes on SiO_2 substrate.[15] As temperature T rises, more phonon modes in the materials are activated and participate into the heat transfer through interfaces. As a result of elevated inelastic phonon interface scattering, both anharmonicity of the atomic interactions and phonon transmission coefficients are enhanced, which then lead to reduction of interfacial thermal resistance, as reported earlier for Si/Ge interfaces.[27]

These results suggest that in practical applications of materials or devices, heat dissipation will depend on the power densities generated by heat sources embedded therein. In this situation, both heat flux across interfaces and local temperature at the heat source increase if the heat cannot be dissipated efficiently. Thus from the conclusion above, the changes in κ_I therein will determined by competition between its dependence on J and T.[9]

Effect of Interlayer Intercalation. In addition to the bulk thermal properties of materials across the interface, that is, 6H-SiC or graphite specifically for our system, the atomic structures

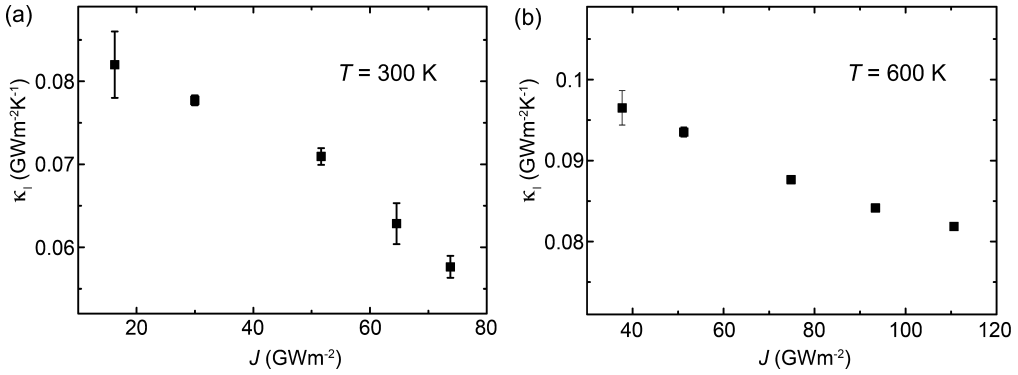

Figure 3. Interfacial thermal conductivity κ_I as a function of the heat flux J across two layers of graphene (between 6H-SiC with buffer carbon layers) at (a) 300 and (b) 600 K, respectively. Error bars show averaged values and standard deviations of κ_I from 3 independent runs.

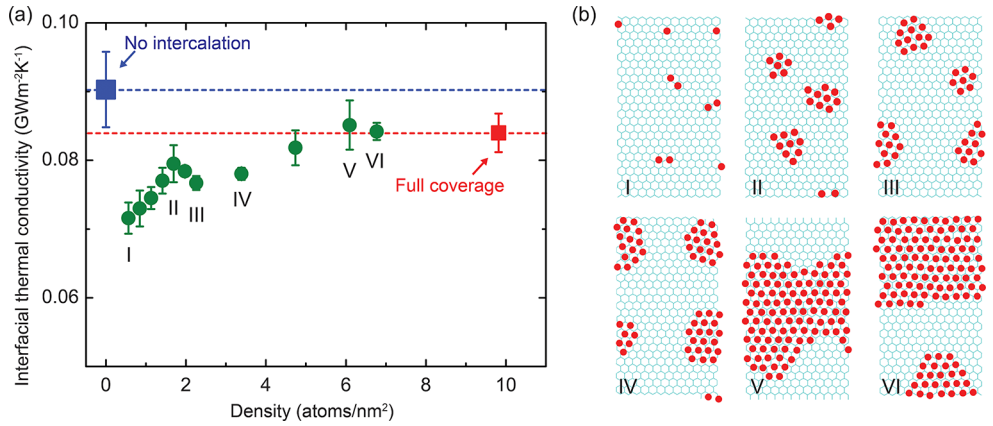

Figure 4. (a) Interfacial thermal conductivity κ_I for graphene layers (N = 2) intercalated with argon atoms, as a function of the areal density. κ_I without intercalation and with full coverage are also plotted here for reference. (b) Snapshots (I–VI) of intercalated argon monolayers as areal density indicated in panel (a), where the underlying graphene lattice and argon atoms are shown in gray lines and red dots respectively. Error bars show averaged values and standard deviations of κ_I from 3 independent runs.

of interfaces could also affect the heat transport process. In order to have a better understanding on it, we further engineer the graphene-6H-SiC interface by tuning its chemistry and explore its effects on the interfacial thermal conductivity.

Recently there have been numerous efforts in functionalizing the interface between graphene and other materials through techniques such as chemical functionalization[28] and intercalation.[29−31] Here we modify the interface by intercalating inert gas molecules into the interlayer space between graphene layers. We choose argon atoms here as an example to illustrate the idea, which could be further generalized to other guest molecules such as oxygen, metals, or polymers. In our model, there are two graphene layers in contact at the interface. We add argon atoms in a two-dimensional random lattice with areal number densities n_{Ar} ranging from 0.5 to 10 nm^{-2}. The simulation methods for the intercalated systems are the same as the one introduced above, that is, NEMD simulations are performed after thermal equilibration. From Figure 4a, we can see that at low concentration, the interfacial thermal conductivity is reduced by the presence of intercalating atoms in comparison with the intercalation-free system. κ_I then rises as the density of argon atoms increases at a low level before n_{Ar} exceeds 1.7 nm^{-2}. Then the interfacial thermal conductivity decreases and increases again by further increasing n_{Ar}. The value of κ_I eventually reaches a saturated value for n_{Ar} higher than 6 nm^{-2}.

This modulation of interfacial thermal conductivity can be explained as follows. By adding argon atoms, a new interface forms with local phonon scatters because of the presence of guest atoms and distortion of original interface structures by them. Thus the interfacial thermal conductivity is reduced. As the areal number density of argon atoms n_{Ar} increases, more contacts form in the new interface, which enhance the interfacial thermal conductivity. As a result, the overall tendency turns upward. The snapshots of intercalating layer of argon atoms showing strong dependence on the areal density are summarized in Figure 4b, which is found to be stable during equilibrium molecular dynamics simulations at a constant temperature T = 300 K. Structural distortion of the graphene sheets locally pin argon atoms and discrete clusters before percolated clusters form at the interface. Distinctly, isolated argon atoms between graphene layers start to cluster for n_{Ar} > 1 atom per nm^2, which subsequently create local structural distortion at the interface and enhanced scattering to thermal flow. The distortion of interfaces and formation of larger contacts compete in this region, resulting in a complicate dependence of κ_I on n_{Ar}, which decreases first, and increases beyond 3 nm^{-2} due to the reduction of distortion by forming larger clusters.

With further increasing of n_{Ar} beyond 4 nm^{-2}, aggregation of argon atoms at elevated areal density results in percolated clusters in the simulated supercell. This could be directly related to changes in interfacial thermal conductivities as

dx.doi.org/10.1021/am3032772 | ACS Appl. Mater. Interfaces 2013, 5, 2599−2603

plotted in Figure 4a. For $n_{Ar} > 6$ nm^{-2}, the interfacial thermal conductivity κ_I of the hybrid graphene-argon interface reaches the value of κ_I at full monolayer coverage of argon atoms, which is only reduced from argon-free interfaces by only 7%. As the intercalated argon atoms insulate the interface electronically, these results suggest that nanoengineering at the graphene-substrate or graphene-metal contacts interfaces could effectively reduce electronic coupling, while maintain the interfacial thermal conductivity κ_I at the same level. Experimental evidence was recently reported that oxygen intercalation is an efficient method for fully decoupling an extended layer of graphene from a metal substrate.[32]

CONCLUSION

In summary, we explore interfacial thermal transfer by considering intercalated graphene layers between 6H-SiC, with focus on the Kapitza conductivities κ_I. Our results show a linear dependence of κ_I on the number of graphene layers, which is explained using a resistor-chain model by including a contact resistance. This model can be used to estimate effective thermal transport behaviors of graphene or graphite-based thermal interface materials and composites. κ_I is also found to increase with environmental temperature and decrease as a function of heat flux, leading to a competitive mechanism when a heat source is embedded.

The interfacial thermal transfer can be engineered by intercalating guest atoms such as argon as explored, which does not change κ_I significantly, but insulates the supported graphene sheet electronically. These results provide basic understanding of interfacial thermal transport and pave the way for future designs of multifunctional thermal interface materials, nanocomposites, and efficient thermal management in nano-electronic devices. The approach could be extended to chemical functionalization and other nanoengineering techniques at the interface for synergetic improvement of thermal, mechanical and electronic performance in materials.

AUTHOR INFORMATION

Corresponding Author

*E-mail: xuzp@tsinghua.edu.cn (Z.X.); peiym@pku.edu.cn (Y.P.).

Notes

The authors declare no competing financial interest.

ACKNOWLEDGMENTS

This work was supported by the National Natural Science Foundation of China through Grant 11222217, 11002079, Tsinghua University Initiative Scientific Research Program 2011Z02174, and the Tsinghua National Laboratory for Information Science and Technology of China.

REFERENCES

(1) Allara, D. L. *Nature* **2005**, *437*, 638.
(2) Dorgan, V. E.; Bae, M.-H.; Pop, E. *Appl. Phys. Lett.* **2010**, *97*, 082112.
(3) Morozov, S. V.; Novoselov, K. S.; Katsnelson, M. I.; Schedin, F.; Elias, D. C.; Jaszczak, J. A.; Geim, A. K. *Phys. Rev. Lett.* **2008**, *100*, 016602.
(4) Nika, D. L.; Pokatilov, E. P.; Askerov, A. S.; Balandin, A. A. *Phys. Rev. B* **2009**, *79*, 155413.
(5) Ghosh, S.; Calizo, I.; Teweldebrhan, D.; Pokatilov, E. P.; Nika, D. L.; Balandin, A. A.; Bao, W.; Miao, F.; Lau, C. N. *Appl. Phys. Lett.* **2008**, *2008*, 151911.
(6) Pop, E.; Varshney, V.; Roy, A. K. *MRS Bull.* **2012**, *37*, 1273.
(7) Xu, Z.; Buehler, M. J. *Nano Lett.* **2009**, *9*, 2065.
(8) Freitag, M.; Steiner, M.; Martin, Y.; Perebeinos, V.; Chen, Z.; Tsang, J. C.; Avouris, P. *Nano Lett.* **2009**, *9*, 1883.
(9) Xu, Z.; Buehler, M. J. *J. Phys.: Condens. Matter* **2012**, *24*, 475305.
(10) Shahil, K. M. F.; Balandin, A. A. *Nano Lett.* **2012**, *12*, 861.
(11) Xu, Z.; Buehler, M. J. *ACS Nano* **2009**, *3*, No. 2767.
(12) Losego, M. D.; Grady, M. E.; Sottos, N. R.; Cahill, D. G.; Braun, P. V. *Nat. Mater.* **2012**, *11*, 502.
(13) Koh, Y. K.; Bae, M.-H.; Cahill, D. G.; Pop, E. *Nano Lett.* **2010**, *10*, 4363.
(14) Hu, L.; Desai, T.; Keblinski, P. *Phys. Rev. B* **2011**, *83*, 195423.
(15) Ong, Z.-Y.; Pop, E. *Phys. Rev. B* **2010**, *81*, 155408.
(16) Tsai, C.-L.; Liao, A.; Pop, E.; Shim, M. *Appl. Phys. Lett.* **2011**, *99*, 053120.
(17) Hao, F.; Fang, D.; Xu, Z. *Appl. Phys. Lett.* **2012**, *100*, 091903.
(18) Plimpton, S. *J. Comput. Phys.* **1995**, *117*, 1.
(19) Müller-Plathe, F. *J. Chem. Phys.* **1997**, *106*, 6082.
(20) Schelling, P. K.; Phillpot, S. R.; Keblinski, P. *Phys. Rev. B* **2002**, *65*, 144306.
(21) Tersoff, J. *Phys. Rev. B* **1989**, *39*, 5566.
(22) Stuart, S. *J. Chem. Phys.* **2000**, *112*, 6472.
(23) Chang, S.; He, J.; Kibel, A.; Lee, M.; Sankey, O.; Zhang, P.; Lindsay, S. *Nat. Nanotechnol.* **2009**, *4*, 297.
(24) Abraham, F. F.; Batra, I. P. *Surf. Sci.* **1989**, *209*, L125.
(25) Berber, S.; Kwon, Y.-K.; Tomanek, D. *Phys. Rev. Lett.* **2000**, *84*, 4613.
(26) Kawamura, T.; Hori, D.; Kangawa, Y.; Kakimoto, K.; Yoshimura, M.; Mori, Y. *Jpn. J. Appl. Phys.* **2008**, *47*, 8898.
(27) Landry, E. S.; McGaughey, A. J. H. *Phys. Rev. B* **2009**, *80*, 165304.
(28) Riedl, C.; Coletti, C.; Iwasaki, T.; Zakharov, A. A.; Starke, U. *Phys. Rev. Lett.* **2009**, *103*, 246804.
(29) Sutter, P.; Sadowski, J. T.; Sutter, E. A. *J. Am. Chem. Soc.* **2010**, *132*, 8175.
(30) Grånäs, E.; Knudsen, J.; Schröder, U. A.; Gerber, T.; Busse, C.; Arman, M. A.; Schulte, K.; Andersen, J. N.; Michely, T. *ACS Nano* **2012**, *6*, 9951.
(31) Si, C.; Zhou, G.; Li, Y.; Wu, J.; Duan, W. *Appl. Phys. Lett.* **2012**, *100*, 103105.
(32) Larciprete, R.; Ulstrup, S.; Lacovig, P.; Dalmiglio, M.; Bianchi, M.; Mazzola, F.; Hornekær, L.; Orlando, F.; Baraldi, A.; Hofmann, P.; Lizzit, S. *ACS Nano* **2012**, *6*, 9551.